Hindawi Publishing Corporation
International Journal of Antennas and Propagation
Volume 2016, Article ID 6075680, 20 pages
http://dx.doi.org/10.1155/2016/6075680

Review Article

Dielectric Resonator Antennas: Basic Concepts, Design Guidelines, and Recent Developments at Millimeter-Wave Frequencies

S. Keyrouz[1] and D. Caratelli[1,2]

[1]*The Antenna Company, High Tech Campus 41, Eindhoven, Netherlands*
[2]*Tomsk Polytechnic University, 84/3 Sovetskaya Street, Tomsk, Russia*

Correspondence should be addressed to S. Keyrouz; shady.keyrouz@antennacompany.com

Received 18 July 2016; Revised 18 September 2016; Accepted 22 September 2016

Academic Editor: Ahmed T. Mobashsher

An up-to-date literature overview on relevant approaches for controlling circuital characteristics and radiation properties of dielectric resonator antennas (DRAs) is presented. The main advantages of DRAs are discussed in detail, while reviewing the most effective techniques for antenna feeding as well as for size reduction. Furthermore, advanced design solutions for enhancing the realized gain of individual DRAs are investigated. In this way, guidance is provided to radio frequency (RF) front-end designers in the selection of different antenna topologies useful to achieve the required antenna performance in terms of frequency response, gain, and polarization. Particular attention is put in the analysis of the progress which is being made in the application of DRA technology at millimeter-wave frequencies.

1. Introduction

The release of the unlicensed 60 GHz band and the development of 5G technologies aimed at increasing data rate on wireless communication network by a factor of 100 [1] will impose stinging specifications (large bandwidth, high gain, small size, and temperature independent performance) on the design of the radio frequency (RF) electronics. Various front-end antenna solutions relying on monopoles, dipoles, and patch antennas have been proposed for millimeter-wave applications. These antennas are characterized by small size, low weight, and low cost and can be easily integrated on chip. However, unless advanced design solutions based on the integration of suitable dielectric superstrates or lensing structures are adopted, these antennas typically suffer from reduced radiation efficiency and narrow impedance bandwidth due to the effect of lossy silicon substrate materials. On the other hand, dielectric resonator antennas (DRAs) are promising candidates to replace traditional radiating elements at high frequencies, especially for applications at millimeter waves and beyond. This is mainly attributed to the fact that DRAs do not suffer from conduction losses and are characterized by high radiation efficiency when excited properly.

DRAs rely on radiating resonators that can transform guided waves into unguided waves (RF signals). In the past, these antennas have been mainly realized by making use of ceramic materials characterized by high permittivity and high Q factor (between 20 and 2000). Currently, DRAs made from plastic material (PolyVinyl Chloride (PVC)) are being realized. The main advantages of DRAs are summarized as follows:

(i) The size of the DRA is proportional to $\lambda_0/\sqrt{\epsilon_r}$ with $\lambda_0 = c/f_0$ being the free-space wavelength at the resonant frequency f_0 and where ϵ_r denotes the relative permittivity of the material forming the radiating structure. As compared to traditional metallic antennas whose size is proportional to λ_0, DRAs are characterized by a smaller form factor especially when a material with high dielectric constant (ϵ_r) is selected for the design.

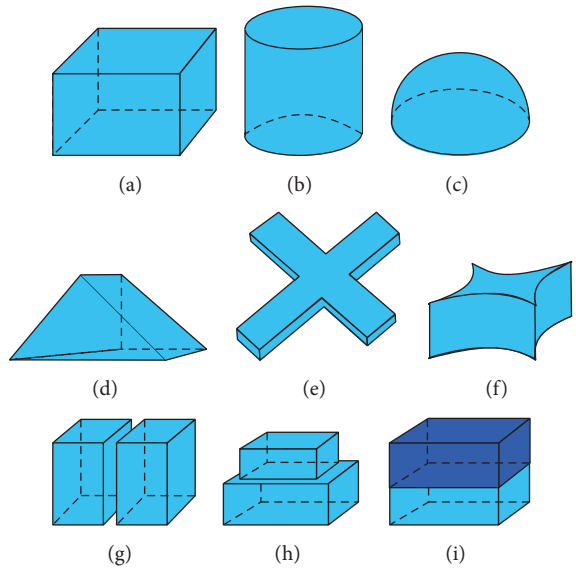

Figure 1: Different radiating structures used for dielectric resonator antennas (DRAs).

(ii) Due to the absence of conducting material, the DRAs are characterized by high radiation efficiency when a low-loss dielectric material is chosen. This characteristic makes them very suitable for applications at very high frequencies, such as in the range from 30 GHz to 300 GHz. As a matter of fact, at these frequencies, traditional metallic antennas suffer from higher conductor losses.

(iii) DRAs can be characterized by a large impedance bandwidth if the dimensions of the resonator and the material dielectric constant are chosen properly.

(iv) DRAs can be excited using different techniques which is helpful in different applications and for array integration.

(v) The gain, bandwidth, and polarization characteristics of a DRA can be easily controlled using different design techniques.

The main target of this paper is to present an up-to-date review study summarizing the most relevant techniques to control circuital characteristics and radiation properties of DRAs. In this way, guidance will be provided to RF front-end designers to achieve the required antenna performance in terms of gain, bandwidth, and polarization. Different geometries of radiating resonators will be discussed first, turning then our attention to advantages and disadvantages of different feeding techniques proposed so far in the literature. Various methodologies that have been used to enhance the impedance bandwidth and the antenna gain will be explored. Furthermore, different techniques to achieve circular polarization are summarized. Finally, the most recent implementation of DRAs on chip and off chip will be presented.

2. Dielectric Resonators

By using a suitable excitation technique, any dielectric structure can become a radiator at defined frequencies. It is to be noticed that, for a given resonant frequency, the size of the dielectric resonator is inversely proportional to the relative permittivity of the constitutive material. The lowest dielectric constant material adopted in DRA design is reported in [2–4], where commodity plastics with relative dielectric constant smaller than 3 have been utilized for the realization of supershaped DRAs.

The basic principle of operation of dielectric resonators is similar to that of the cavity resonators [5] and is thoroughly discussed in literature. The most two popular radiating dielectric resonators are the cylindrical and the rectangular ones. They will be reviewed in this section. Design equations to calculate the relevant resonant frequencies are given. More complex dielectric resonators, such as the spherical/hemispherical, cross-shaped, and supershaped (see Figure 1) ones, will be also discussed in this section.

2.1. Cylindrical DRA. Cylindrical DRAs have been studied extensively in literature. Figure 2 shows the three-dimensional view (a) and the cross-sectional view (b) of a probe-fed cylindrical DRA. The antenna consists of a cylindrical dielectric resonator (DR) with height h, radius a, and dielectric constant ϵ_r. The DR is placed on top of a ground plane and fed by a coaxial connector. The main advantages of the cylindrical DRA consist in the ease of fabrication and the ability to excite different modes.

The resonant frequency of the modes supported by a cylindrical DRA can be calculated using the following equations [6]:

$$f_{\mathrm{TE}_{npm}} = \frac{c}{2\pi\sqrt{\epsilon_r\mu_r}}\sqrt{\left(\frac{X_{np}}{a}\right)^2 + \left(\frac{(2m+1)\,\pi}{2h}\right)^2}, \quad (1)$$

$$f_{\mathrm{TM}_{npm}} = \frac{c}{2\pi\sqrt{\epsilon_r\mu_r}}\sqrt{\left(\frac{X'_{np}}{a}\right)^2 + \left(\frac{(2m+1)\,\pi}{2h}\right)^2}, \quad (2)$$

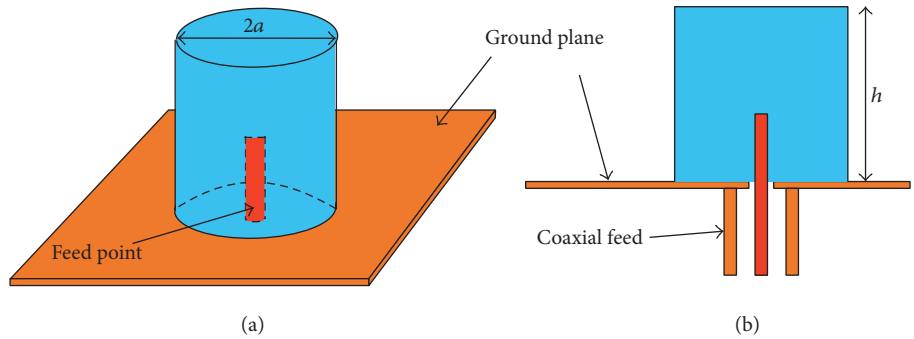

Figure 2: Three-dimensional (a) and cross-sectional view (b) of the probe-fed cylindrical DRA.

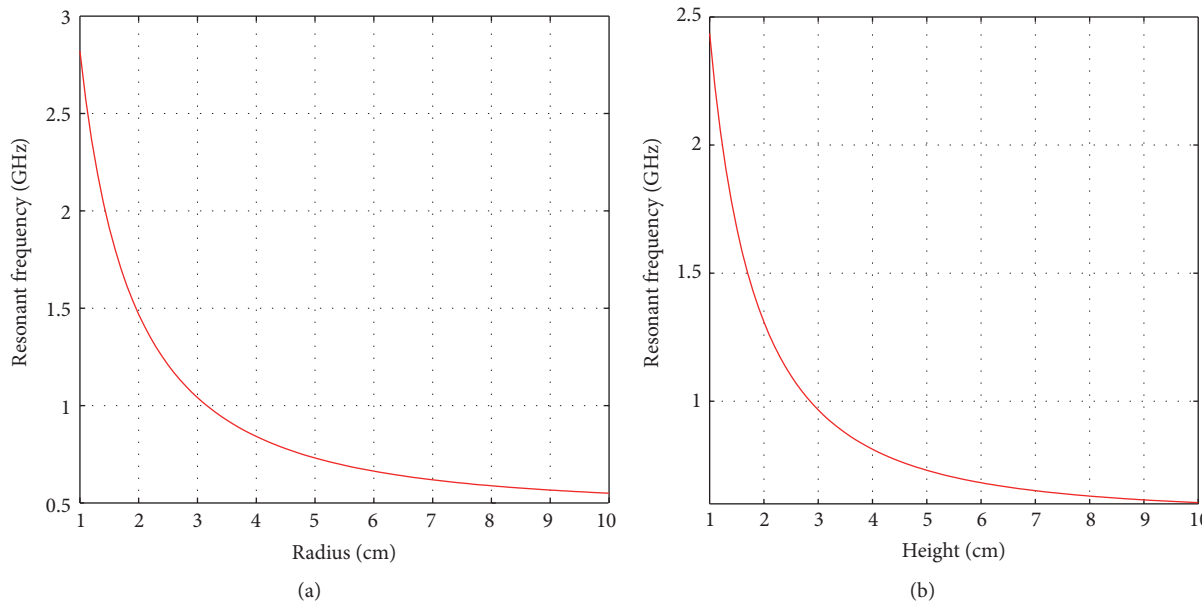

Figure 3: Resonant frequency as a function of the radius (a) and height (b) of a cylindrical DRA with relative permittivity $\epsilon_r = 10$.

Table 1: Roots of the Bessel functions of the first kind, X_{np}.

p	n				
	$n = 1$	$n = 2$	$n = 3$	$n = 4$	$n = 5$
$p = 0$	2.404	5.520	8.653	11.791	14.930
$p = 1$	3.831	7.015	10.173	13.323	16.470
$p = 2$	5.135	8.417	11.619	14.795	17.959

Table 2: Roots of the first-order derivative of the Bessel functions of the first kind, X'_{np}.

p	n				
	$n = 1$	$n = 2$	$n = 3$	$n = 4$	$n = 5$
$p = 0$	3.831	7.015	10.173	13.323	16.470
$p = 1$	1.841	5.331	8.536	11.706	14.863
$p = 2$	3.054	6.706	9.969	13.170	16.347

where X_{np} and X'_{np} denote the roots of the Bessel functions of the first kind and of the relevant first-order derivatives, respectively (see Tables 1 and 2).

The impact of the geometrical parameters of a cylindrical DRA (radius and height) as well as of the relative dielectric constant (ϵ_r) on the resonant frequency is investigated. Equation (2) is used to calculate the resonant frequency of the fundamental model TM_{110} of the cylindrical DRA. Figure 3 shows the resonant frequency as a function of the DRA's radius (see Figure 3(a)) and as a function of the DRA's height (see Figure 3(b)). The dielectric constant used to calculate the resonant frequencies is set to $\epsilon_r = 10$. It is indicated in the figures that the resonant frequency decreases by increasing either the radius or the height or both of them simultaneously.

Figure 4 shows the effect of the relative dielectric constant (ϵ_r) on the resonant frequency. It can be noticed that the resonant frequency of the fundamental mode decreases by increasing the dielectric constant of the DRA. This behavior is the most important characteristic of the DRA since it allows decreasing the size of the DRA by increasing its dielectric constant. It is to be noted that the impedance bandwidth is inversely proportional to the relative permittivity of the DR.

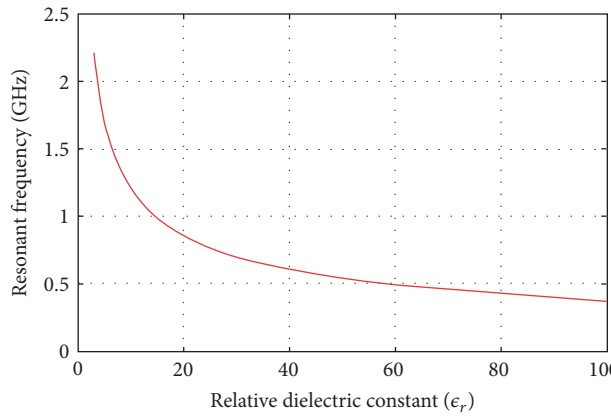

FIGURE 4: Resonant frequency of a cylindrical DRA with radius $a = 2.5$ cm and height $h = 5$ cm as a function of the relative dielectric constant.

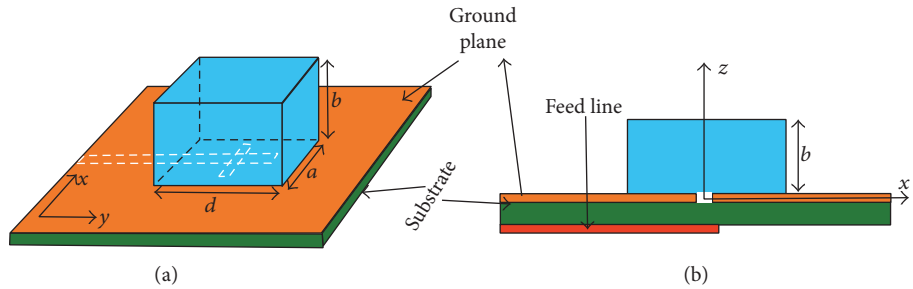

FIGURE 5: Three-dimensional view (a) and cross-sectional view (b) of an aperture-fed rectangular DRA.

Therefore, the use of materials with high dielectric constant can result in a narrowband antenna behavior.

2.2. Rectangular DRA. Figure 5 shows the three-dimensional and cross-sectional views of a rectangular DRA fed by a slot aperture. The rectangular DRA consists of a rectangular dielectric resonator with relative dielectric constant ϵ_r. The dimensions of the rectangular DR are $a \times d \times h$ (width × length × height).

The main advantage of the rectangular DRA is that it is characterized by three independent geometrical dimensions, a, b, and d (see Figure 5(a)); this offers more design flexibility as compared to the cylindrical DRA. Furthermore, the rectangular DRA is characterized by low cross-polarization level as compared to the cylindrical DRA [7].

The dielectric waveguide model [8] is used to analyze the rectangular DRA. When the DRA is mounted on a ground plane, TE modes are excited. The resonant frequency of the fundamental mode, TE_{111}, is calculated by means of the following equations [9]:

$$f_0 = \frac{c}{2\pi\sqrt{\epsilon_r}}\sqrt{k_x^2 + k_y^2 + k_z^2},$$

$$k_x = \frac{\pi}{a},$$

$$k_z = \frac{\pi}{2b},$$

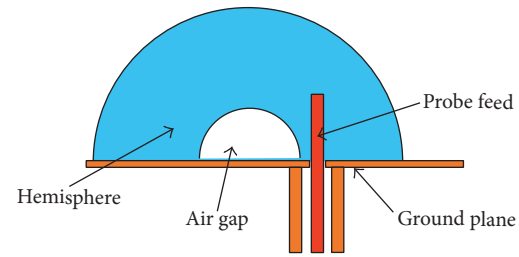

FIGURE 6: Probe-fed hemispherical DRA with an air gap for bandwidth enhancement as suggested in [10].

$$d = \frac{2}{k_y}\tanh\left(\frac{k_{y0}}{k_y}\right), \quad k_{y0} = \sqrt{k_x^2 + k_z^2}, \tag{3}$$

where ϵ_r is the relative dielectric constant of the material forming the resonator.

2.3. Hemisphere and Cross-Shaped and Supershaped DRAs. In this section attention is put also on the hemisphere and the cross-shaped and the supershaped DRAs.

A probe-fed hemispherical DRA with an air gap of hemispherical shape between the dielectric structure and the ground plane is presented in [10] and is shown in Figure 6. It has been found that, by incorporating this gap, the DRA achieves an impedance bandwidth which is nearly twice that

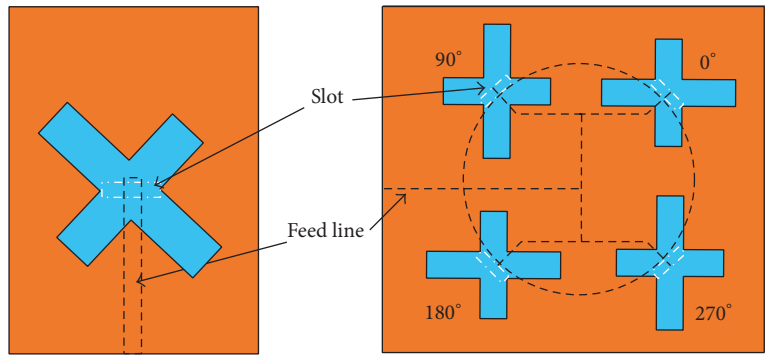

Figure 7: Cross-shaped DRA (a) and a sequentially fed cross-shaped DRA array (b) as suggested in [12].

without an air gap. A dedicated section summarizing the most relevant techniques to improve the impedance bandwidth will be presented later in the paper.

The authors in [11] demonstrated for the first time the possibility of using glass dielectric resonators as light covers. A dual-band hollow and solid hemispherical glass DRAs are presented in [11]. The hollow hemisphere is excited by a slot while the solid one is a probe-fed DRA. By taking advantage of the transparency of the glass an LED was inserted into the air gap through the ground plane resulting in a DRA that can be used as a light cover. It has been demonstrated in the paper that the insertion of an LED inside the DRA (for both solid and hollow DRA) has a negligible effect on the antenna performance.

The cross-shaped dielectric resonator is mainly suggested to design circularly polarized antenna. A cross-shaped DRA as suggested in [12] is shown in Figure 7(a). To achieve a wide-band circular polarization bandwidth the cross DRA should be rotated 45° with respect to the slot and the length of the arms should be optimized [12]. The individual cross-shaped DRA supports a circular polarization bandwidth of 5% with an axial ratio less than 3 dB. In addition to the circular polarization (CP), the measured impedance bandwidth of the cross DRA reaches 16% at 10 dB return-loss level [12].

In order to achieve higher impedance bandwidth and larger circular polarization bandwidth, a sequentially fed array of cross DRA is proposed in the same paper as shown in Figure 7(b). In this way, the impedance bandwidth and the CP bandwidth are increased to 25% and 15%, respectively.

Recently, a very similar concept has been adopted in [13] to design an mm-wave DRA. The presented design consists of a four-by-four array of sequentially fed rectangular dielectric resonators excited by a cross-shaped slot in order to achieve circular polarization. The simulated impedance bandwidth extends from 26.9 GHz to 33.7 GHz, whereas the simulated axial ratio bandwidth at 3 dB level extends from 24.1 GHz to 31.1 GHz.

A plastic-based supershaped DRA has been presented in [2–4] and is shown in Figure 8. The reported impedance bandwidth is extended to 74% by using a supershaped dielectric resonator.

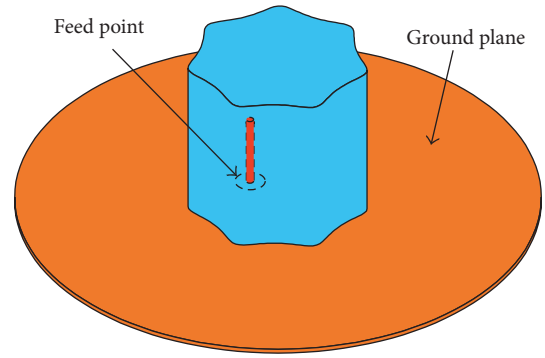

Figure 8: Probe-fed supershaped DRA [2].

The main advantage of the presented supershaped DRA is that it uses plastic (PolyVinyl Chloride (PVC)) as dielectric material which makes it very cost effective and easily manufacturable.

In addition to the basic dielectric resonators that have been discussed in this section, numerous attempts have been performed to combine different dielectric resonators together in order to optimize antenna performance. Figures 1(d), 1(e), and 1(f) show different configurations of combined DRAs. The advantages of combining different DRs will be presented later in the paper but first different feeding structures of DRAs will be discussed in the following section.

3. Feeding Structures

One of the main advantages of DRA technology is that various feeding techniques can be used to excite the radiating modes of a dielectric resonator.

3.1. Probe-Fed DRA. The probe-fed DRA is among the first reported DRAs [10, 14] and is shown in Figure 9. In this configuration, the DR is directly disposed on the ground plane and is excited by a coaxial feed through the substrate. The coaxial probe can either penetrate the DR (see Figure 9(a)) or can be placed adjacent to the DR as shown in Figure 9(b).

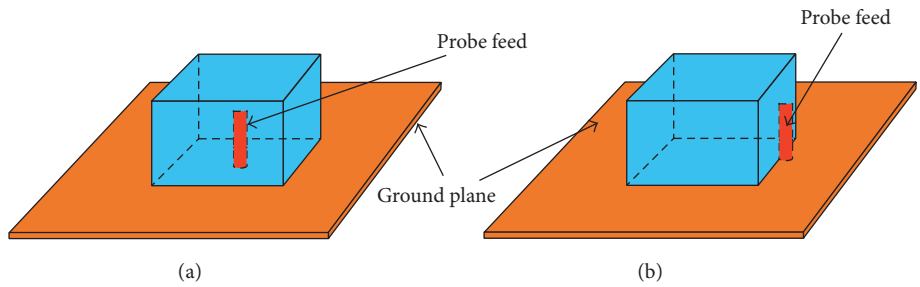

Figure 9: Probe-fed rectangular DRA.

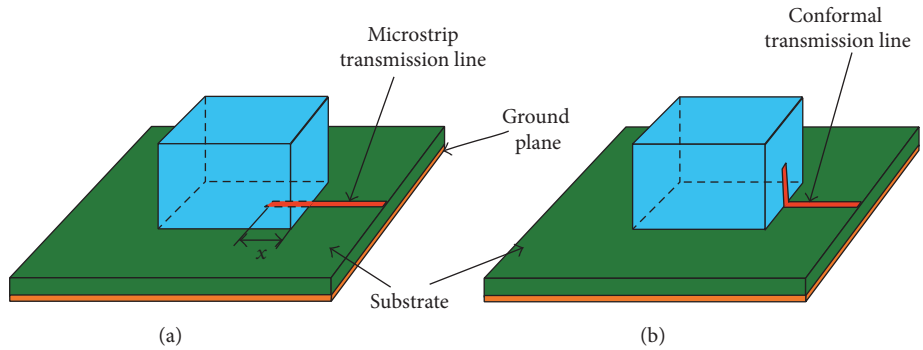

Figure 10: Three-dimensional view of conventional (a) and conformal (b) microstrip transmission line feeding networks.

By optimizing length and position of the feeding probe, the input impedance of the DRA can be tuned [15] and, consequently, the resonance frequency can be controlled. The main benefit associated with a probe penetrating the DRA (see Figure 9(a)) is that it provides high coupling to the DR which, in turn, results in high radiation efficiency. The main drawback of such configuration is that a hole needs to be drilled in the DRA. The dimensions of the drilled hole need to match the dimensions of the probe (length and radius) otherwise the effective dielectric constant of the resonator will be affected, this causing a shift in the resonance frequency of the antenna. It is to be noticed, furthermore, that drilling a hole in the DR complicates the manufacturing process and makes it more expensive.

A reduced manufacturing complexity is achieved by placing the excitation probe adjacent to the DR (see Figure 9(b)). This technique is cost-effective but results in a smaller coupling to the DR, which eventually affects the radiation characteristics of the structure.

For high-frequency applications where the antenna is manufactured on a Printed Circuit Board (PCB), or is directly integrated on chip, probe-fed DRAs are not practical.

3.2. Microstrip Transmission Line-Fed DRA. Another way to feed the DRA is by using printed transmission lines. Figure 10 shows the three-dimensional view of a rectangular DRA fed by a microstrip line (see Figure 10(a)) and by a conformal transmission line (see Figure 10(b)). In conventional microstrip line-fed DRAs, the dielectric resonator is directly placed on the transmission line that is printed on the PCB substrate. One of the first reported DRAs fed by a microstrip line is reported in [16]. It has been shown in [16] that the overlap distance x (see Figure 10(a)) determines the coupling strength and the specific mode that is excited by the transmission line. The strongest coupling occurs when x is slightly shorter than one-quarter of a dielectric wavelength of the resonance frequency. The main drawback of the microstrip transmission line feed is that the feeding line is not isolated from the dielectric resonator which can affect the radiation performance of the DRA. In addition, when placing the dielectric resonator directly on the top of a transmission line, an undesired air gap is created between the resonator and the substrate of the PCB.

In a conformal transmission line-fed DRA, the resonator is placed directly on the PCB substrate and the feeding microstrip is bent over the resonator as shown in Figure 10(b). By using this configuration, the input transmission line is integrated with the DR without creating an air gap. The shape of the transmission line that is bent over the dielectric resonator can be optimized to improve the performance of the DRA. As an example, a conformal elliptical patch that feeds an U-shaped DRA is suggested in [17] where an impedance bandwidth of 72% is achieved.

3.3. Coplanar-Waveguide-Fed DRA. The coplanar waveguide excitation was first introduced in [18], where a coplanar waveguide (CPW) circular-loop network that feeds a cylindrical DRA is presented. A rectangular DRA fed by a similar structure is shown in Figure 11(a). The main advantage of the CPW excitation is that the coupling slot that is underneath the dielectric resonator can be modified to optimize the performance of the DRA. In [19] the circular-loop feeding

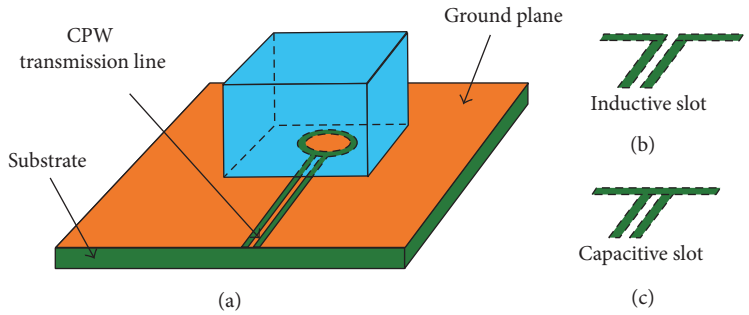

Figure 11: Rectangular DRA fed by a CPW circular-loop network (a). Inductive slot feed (b). Capacitive slot feed (c).

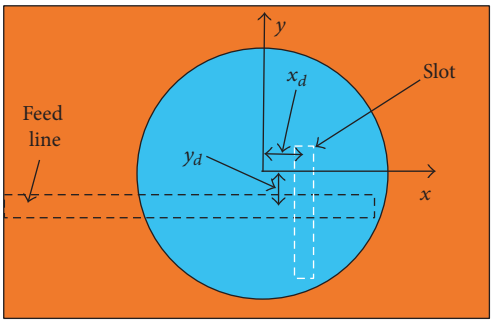

Figure 12: Top view of an aperture-coupled hemispherical DRA as presented in [20].

network is replaced by an inductive slot (see Figure 11(b)) and by a capacitive slot (see Figure 11(c)) in combination with a hemispherical DRA. It has been shown that the capacitive slot provides an additional resonance which results in a dual-band behavior, with two resonances associated with the DR and the feeding slot itself, respectively. CPW feeding structures are widely used for millimeter-wave applications especially when the DRA is integrated in a system on chip (SoC). As a matter of fact, by using CPW transmission lines, it is possible to achieve high antenna efficiency since the ground plane separates the dielectric resonator from the lossy silicon substrate.

3.4. Slot-Fed DRA. The most popular feeding technique for DRAs is via a slot in the ground plane. This excitation method is known as aperture coupling. The guided wave propagating along the transmission line is coupled, through the slot, to the resonant modes of the DR.

Figure 12 shows the top view of an aperture-coupled hemispherical DRA as presented in [20]. The effect of the slot displacements x_d and y_d (see Figure 12) from the center of the DRA is investigated in [20]. It has been found that best resonance (impedance matching) is achieved when the DR is perfectly centered on top of the slot ($x_d = y_d = 0$). The main advantage of this method is that it avoids a direct electromagnetic interaction between the feed line and the DRA as indicated in Figure 13. By using this topology, the spurious radiation from the feeding network can be reduced, thus enhancing the polarization purity of the DRA. The drawback of such excitation method is that the slot length

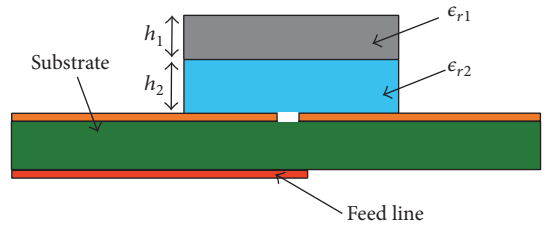

Figure 13: Cross-sectional view of a two-layer rectangular DRA for size reduction as suggested in [21].

should be around $\lambda/2$ which is a challenge to realize at lower frequencies while keeping the size of the DRA compact.

4. DRA Size Reduction Methods

The two most common techniques to minimize the size of a DRA are either to use material with high dielectric constant or to insert a metal plate in the symmetry plane of the DR. These techniques are reviewed in this section.

4.1. High Relative Dielectric Constant (ϵ_r). In general, the size of the DRA is inversely proportional to the dielectric constant (ϵ_r) of the resonator as seen in Figure 4. So in order to decrease the size of the DRA, a material with a high dielectric constant can be chosen; however, this should be carefully done since the impedance bandwidth can be affected negatively by the choice of the dielectric material. In [9] a low-profile rectangular DRA ($0.026\lambda_0$) with very high relative

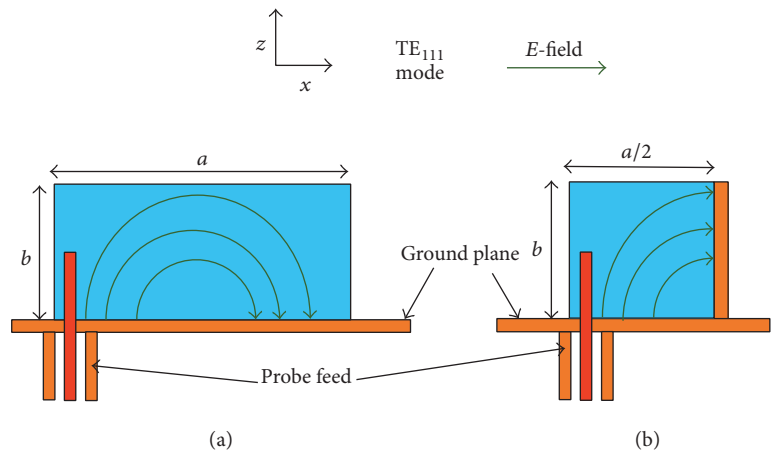

Figure 14: Cross-sectional view of a probe-fed rectangular DRA (a) and its miniaturized version (b) by placing a conducting plate at $x = a/2$.

permittivity ($\epsilon_r = 100$) is presented. It is demonstrated that, even when using such a high dielectric constant material, a reasonable impedance bandwidth of 1.1% to 3.3% can be achieved.

To overcome the limitation related to reduced bandwidth a multilayer DRA topology can be adopted. By optimizing the dielectric constant and height of each layer, the DRA parameters (size, impedance bandwidth, and gain) can be controlled and optimized. Figure 13 shows the cross-sectional view of a two-layer rectangular DRA as suggested in [21]. This configuration offers additional degrees of freedom (ϵ_{r2} and h_2) in the design of a DRA as compared to the single-layer antenna configuration. Using this methodology, the authors in [21] were able to design a low-profile rectangular DRA (having height of $0.1\lambda_0$) with an impedance bandwidth of 40% and an average gain of 9 dBi.

4.2. Metal Plate along Symmetry Plane. The second design technique to minimize the size of a DRA consists in the integration of metal plates along the relevant symmetry planes, as it easily follows from the application of image theory [22]. Figure 14(a) shows the cross-sectional view of a probe-fed rectangular DRA with length a and height b. Its corresponding miniaturized version is shown in Figure 14(b).

As indicated in the figure, the size of the DRA can be halved by placing a conducting plate along the central cross-section of the dielectric resonator at $x = a/2$. The effect of the miniaturization on the resonant frequency and the impedance bandwidth of a DRA was investigated in [23] and the results are summarized in Table 3. The dimensions, a and b, listed in the table are specified in accordance with Figure 14. One can clearly notice that the insertion of the metal plate allows halving the volume of the DRA but, at the same time, results in a reduction of the available impedance bandwidth by a factor of three. It should be mentioned that when a conducting plate is used, the position as well as the length of the feeding probe should be fine-tuned in order to match the input impedance of the antenna at the desired resonant frequency.

Table 3: Effect of the miniaturization of a rectangular DRA [23].

a (mm)	b (mm)	Volume (cm^3)	ϵ_r	Conducting plate	f_0 (GHz)	Impedance bandwidth
88	40	70.4	12	No	1.22	16%
44	40	35.2	12	Yes	0.918	5.4%

Table 4: Measured gain of a DRA with and without SMSH [25].

Frequency (GHz)	5.8	5.9	6.0	6.1	6.2
Gain without SMSH (dBi)	1.4	2.8	3.8	4.2	2.7
Gain with SMSH (dBi)	7.9	8.8	8.2	8.2	6.9

Similarly, the size of a cylindrical DRA can be reduced by 75% by placing a Perfect Electric Conductor (PEC) and a Perfect Magnetic Conductor (PMC) at the symmetry planes of cylinder, as shown in [24].

5. DRA Gain Enhancement Methods

The most straightforward approach to increase the gain of a DRA is by arraying individual DRAs. The gain of a DRA array increases by increasing the number of DR elements in the array. However this approach is not the main goal of this section. Attention is put here on two alternative techniques to enhance the gain of a single DRA element.

5.1. Integration of Additional Structures. An efficient way to increase the gain of a DRA relies on the integration of additional structures useful to focus the antenna radiation in one direction and increase, in this way, its gain. A straightforward example of such design approach is the surface mounted short horn (SMSH) DRA presented in [25]. A cross-sectional view of the SMSH is shown in Figure 15.

The suggested DRA consists of a slot-fed rectangular dielectric resonator with four additional inclined metallic plates used to form a horn-like structure. The effect of the SMSH structure on the DRA gain is quantified in Table 4. The figures of merit listed in the table are taken from [25].

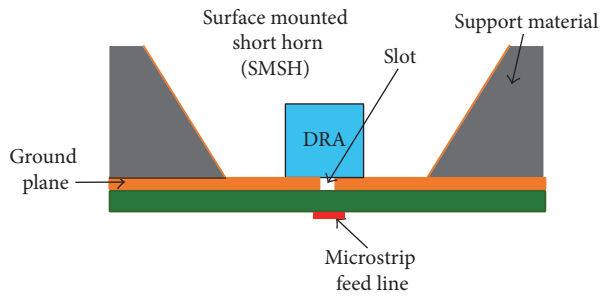

Figure 15: A surface mounted short horn (SMSH) configuration as suggested in [25].

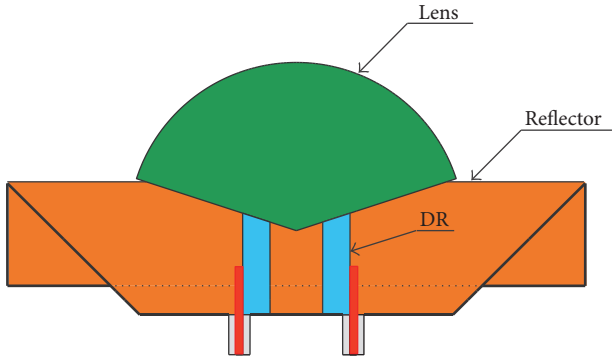

Figure 16: High-gain mushroom-shaped DRA structure as presented in [27].

It can be noticed that the addition of the SMSH results in a 4.4 dB increase of the antenna gain at 6 GHz. The same approach has been used in [26] where a cylindrical DRA integrated on a periodic substrate composed of circular metal strips is presented. By optimizing the distribution of the strips around the DRA a 3 dB enhancement of the antenna gain at the design frequency has been achieved.

Recently a high-gain mushroom-shaped DRA has been presented in [27]. The suggested design is shown in Figure 16 and consists of a probe-fed hollow cylindrical DRA. A spherical-cap lens is placed on top of the cylindrical DRA to increase the antenna gain. It has been shown that the addition of the lens on top of the cylinder will increase the gain by 3 dB to 5.8 dB. The front-to-back ratio is increased between 4.6 dB and 8.8 dB across the operational frequency band. In addition to the lens, the suggested cylindrical DRA is surrounded by a metal truncated-cone reflector. The measured antenna gain of the suggested DRA is larger than 10 dBi between 4.5 GHz and 9.5 GHz with a maximum of 16 dBi around 8.5 GHz.

5.2. Excitation of Higher-Order Modes. The second method to increase the gain of an individual DRA is by exciting the relevant higher-order modes, thus making the DRA electrically larger with respect to its fundamental resonant frequency. It has been shown in [28] that when the $TE_{\delta 15}$ mode of the rectangular DRA is excited, a 6 dB increase of the antenna directivity is achieved as compared with the directivity obtained when exciting the fundamental resonant mode ($TE_{\delta 11}$).

The design of a pattern-reconfigurable cylindrical DRA with high gain resulting from the excitation of higher-order $HEM_{21(1+\delta)}$ modes has been reported in [29].

Recently, a cylindrical DRA with a measured peak gain of 11.6 dBi has been reported in [30]. In this design, the higher-order HEM_{133} mode of a cylindrical dielectric resonator is excited in order to achieve the desired antenna performance.

6. Circular Polarization

One of the advantages of DRAs is that their polarization can be easily controlled. In this section different techniques to design circularly polarized DRAs are reviewed.

6.1. Dual-Feed Excitation. Exciting a DRA by using two ports with a 90° phase shift is a simple but effective means for achieving circular polarization of the radiated electromagnetic field. Figure 17 shows a probe-fed cylindrical DRA relying on the mentioned approach [31]. The measured axial ratio along the broadside direction of this antenna has been reported to be 0.45 dB, thus indicating a very good circular polarization property.

The same design strategy has been applied in [32], where a cylindrical DRA is excited by two conformal microstrip transmission lines. The suggested design offers a 3 dB axial ratio bandwidth of 40%.

6.2. Single-Feed Excitation. Circularly polarized DRAs can be designed also by using a single feed placed at a location where two orthogonal modes can be excited. This technique has been applied in [33] in combination with a circular sector dielectric resonator. The probe feed is placed between the center of the sector (where the $TM_{21\delta}$ is excited) and the edge of the sector (where the $TM_{11\delta}$). A 3 dB axial ratio bandwidth of 10% has been measured for the DRA presented in [33].

In order to achieve circular polarization in slot-fed DRAs, the dielectric resonator and the feeding slot are to be properly rotated relative to each other, so that two orthogonal modes can be excited with the desired phase difference. Figure 18 shows the cross-sectional view (a) and the top view of a slot-fed rectangular DRA. As indicated in Figure 18(b), the DRA is rotated with an angle ϕ with respect to the slot. When $\phi = 45°$ two orthogonal modes with 90° phase differences can be excited which results in a circularly polarized pattern. This technique has been used in [34, 35] to design circularly polarized rectangular DRAs with a 3 dB axial ratio bandwidth of 1.8% and 3%, respectively. The same strategy has been used in [12] to excite the cross-shaped DRA shown in Figure 7.

A novel circularly polarized three-layer stacked DRA has been presented in [36]. Each layer is made out of a homogeneous dielectric material with relative permittivity $\epsilon_r = 10.7$ and rotated by an angle of $\phi = 30°$ relative to the adjacent one. In this way, a 3 dB axial ratio bandwidth of 6% has been obtained, in combination with a wide impedance bandwidth of 21%.

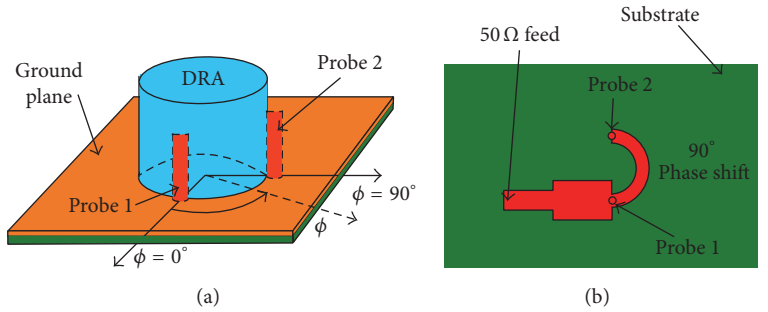

Figure 17: Circularly polarized dual-fed cylindrical DRA as suggested in [31].

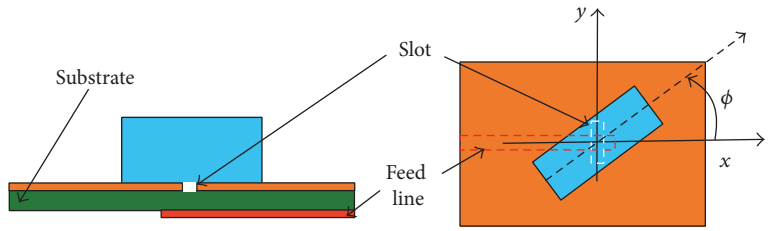

Figure 18: Cross-sectional view (a) and top view (b) of a rotated rectangular DRA as suggested in [34, 35].

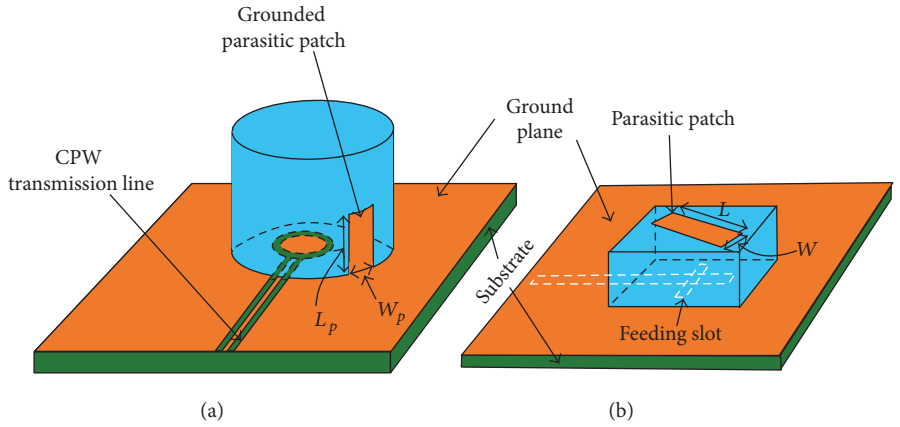

Figure 19: Three-dimensional view of a cylindrical DRA with a grounded parasitic patch (a) as introduced in [40] and three-dimensional view of a rectangular DRA with a parasitic patch placed on its top face (b) as presented in [39].

Instead of rotating the DR itself, location and geometry of the feeding slot can be optimized in order to achieve circular polarization. This technique has been used in [37, 38] where cross-shaped slots have been proposed for the mentioned design goal. In particular, the dual-band circularly polarized rectangular DRA presented in [37] features measured 3 dB axial ratio bandwidths of 9.7% and 20%, respectively, in the two operational frequency ranges. In [38], an offset cross-shaped slot has been used to excite a cylindrical DRA, thus achieving a measured 3 dB axial ratio bandwidth of 4.6%.

6.3. Single-Feed Excitation with Parasitic Metal Strip. Another method for exciting two orthogonal modes and enforcing a circular polarization of the radiated electromagnetic field relies on the use of parasitic metal strips/patches attached to the surface of the dielectric resonator. The parasitic metallic element introduces an asymmetry in the DRA structure which eventually leads to the excitation of two orthogonal modes with the desired phase difference [39]. The parasitic patch can be as shown in Figure 19(a) or kept floating on the top of the DRA as shown in Figure 19(b). An example of circularly polarized rectangular DRA with floating parasitic metal strip placed on its top face is reported in [39]. By adjusting the width, W, and length, L, of the strip (see Figure 19(b)), the axial ratio of the antenna can be easily tuned. By virtue of this design approach, a 2 dB axial ratio bandwidth of 6% can be achieved.

A circularly polarized cylindrical DRA with grounded parasitic strip has been presented in [40] and shown in

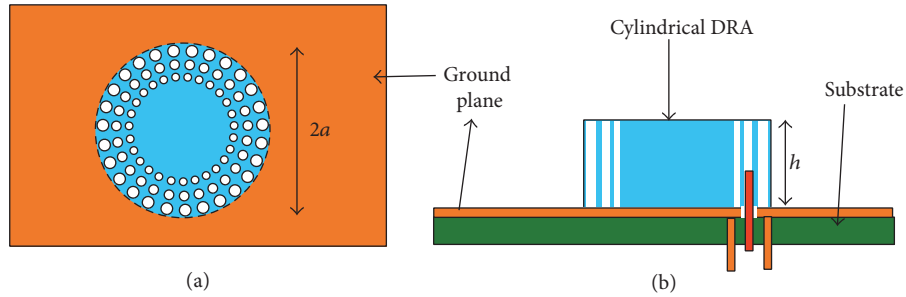

Figure 20: Top (a) and cross-sectional view (b) of a perforated DRA as suggested in [46].

Figure 19(a). It has been demonstrated that the location of the parasitic patch is not very critical for the purity of the circular polarization (see Figure 19(a)). On the other hand, the axial ratio of the antenna is strongly affected by the length of the patch, L_p, whereas the width of the parasitic patch, W_p, plays a none significant role. By tuning L_p and W_p the polarization properties of the DRA can be tuned. Similar conclusions have been reported in [41] where a rectangular DRA with grounded parasitic patch has been investigated.

7. Impedance Bandwidth Enhancement Methods of DRAs

In this section, different techniques useful to broaden the impedance bandwidth of a DRA are summarized.

7.1. Combining Different Dielectric Resonators. Dielectric resonators can be combined together to broaden the impedance bandwidth of the resulting DRA structure. Figures 1(g), 1(h), and 1(i) show different configurations of combined DRAs. By placing multiple dielectric resonators of different dimensions on top of each other (see Figure 1(h)), different modes can be excited. In this way, dual-band or broadband behavior can be achieved. By using such approach, a staircase-shaped DRA has been designed and presented in [42, 43]. A 10 dB return-loss impedance bandwidth of 36.6%, from 7.56 GHz to 10.95 GHz, has been obtained by using the three-step staircase-shaped DRA proposed in [42]. A very similar configuration consisting of a two-step staircase-shaped probe-fed DRA has been presented in [44]. The measured impedance bandwidth of the suggested design is 44% and covers a frequency range from 7.45 GHz to 11.6 GHz. Recently, a dual-band circular DRA with staircase geometry has been proposed in [45].

An alternative design approach, useful to achieve large impedance bandwidths, consists in the tapering of the permittivity distribution within the DR. This can be done either by combining multiple layers with different dielectric constants or by drilling holes of different diameters into the DR in order to taper the effective permittivity of the structure. The geometry of a perforated DRA is shown in Figure 20. This concept has been investigated in [46], where an impedance bandwidth of 26.7% ($\epsilon_r = 10.2$) has been reported.

Dual-band or wide-band characteristics can be easily synthesized by exciting different resonant modes in multilayered DRAs consisting of different dielectric laminates with properly selected permittivity. A cross-sectional view of a two-layer DRA is shown in Figure 13. It has been shown that when ϵ_{r2} (dielectric constant of the bottom layer) is smaller than ϵ_{r1} (dielectric constant of the top layer), an impedance bandwidth of 40% at 10 dB return-loss level can be obtained [21]. Based on these findings, the antenna impedance bandwidth can be further broadened by using an air gap ($\epsilon_{r2} = 1$) as bottom layer [47, 48]. Both DRAs presented in [47, 48] are fed by a tapered strip printed on one side of the dielectric resonator, the relevant impedance bandwidth being of 120% (2.6–11 GHz) and 96% (2.13–6.08 GHz), respectively.

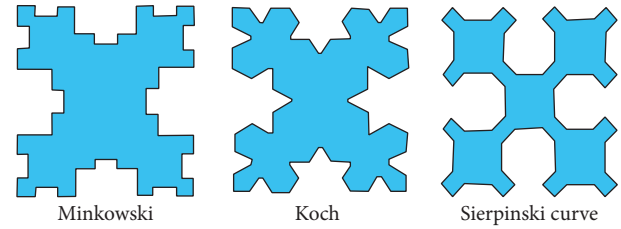

Figure 21: Different fractal boundary structures proposed and simulated in [50].

An alternative antenna topology that can feature wide impedance bandwidth or dual-band operation is the one consisting of two dielectric resonators next to each other and separated by a gap, as shown in Figure 1(g). This design approach has been suggested in [49] where two rectangular DRs are placed on the top of edges of the feeding slot produced in the antenna ground plane. By optimizing the dimensions of the dielectric resonators, the desired dual-band or wide-band behavior can be synthesized.

7.2. Shaping the Dielectric Resonator. When shaping the dielectric resonator, different modes can be excited and, in this way, a wide impedance bandwidth achieved. A U-shaped DRA ($\epsilon_r = 9.8$), fed by means of a conformal elliptical patch, has been proposed in [17]. The suggested design offers a 72% impedance bandwidth in the frequency range between 3.82 GHz and 8.12 GHz.

A CPW-fed fractal DRA topology has been proposed in [50] in order to excite higher-order modes with quasi-degenerate resonant frequencies resulting in a wide impedance bandwidth. Different fractal DRAs, with Minkowski, Koch, and Sierpinski profiles, have been investigated in [50] (see Figure 21). The numerically predicted characteristics

Table 5: Numerically Simulated Characteristics of fractal-based DRAs as Reported in [50].

DRA profile	Resonant frequency (GHz)	Impedance bandwidth (MHz)	Gain (dBi)
Minkowski	6.59	2870	4.12
Koch	6.8	2540	3.51
Sierpinski curve	8.0	1610	1.05

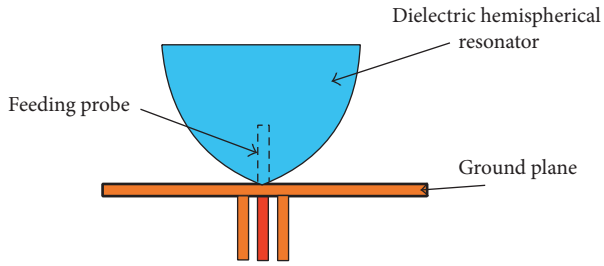

Figure 22: Cup-shaped inverted hemispherical DRA as suggested in [51] for impedance bandwidth enhancement.

of the mentioned fractal-based DRAs are summarized in Table 5. One can notice that the Minkowski DRA features the highest gain and largest impedance bandwidth as compared to the Koch and Sierpinski ones. The simulated results for the Minkowski DRA have been verified by experimental measurements, and in this way an impedance bandwidth of 64% (from 5.52 GHz to 10.72 GHz) has been demonstrated.

An alternative antenna topology that provides a large impedance bandwidth is the supershaped DRA shown in Figure 8. By optimizing the shape of the DRA an impedance bandwidth of 74% (from 6.7 GHz to 14 GHz) has been achieved. To this end, a plastic-based dielectric resonator having relative permittivity $\epsilon_r = 2.73$ has been used [2].

Finally, the cup-shaped inverted hemispherical DRA design presented in [51] is to be mentioned in this survey. The configuration of the suggested DRA is shown in Figure 22. The impedance bandwidth of such DRA is 83% around the central resonant frequency of 2.3 GHz. The permittivity of the dielectric material adopted for the manufacturing of said antenna is $\epsilon_r = 9.2$.

7.3. Effect of the Feeding Slot. In order to increase the impedance bandwidth of an aperture-fed DRA, an annular slot can be used as proposed in [40, 52]. The configuration of the annular slot is shown in Figure 23. Using this solution, the impedance bandwidth can be increased to 18%, while using a dielectric material with relative permittivity $\epsilon_r \simeq 10$.

The annular slot-based approach has been extended in [53], becoming a circular aperture excited by a microstrip line with fork-like tuning stub. The configuration of the feeding network and the circular aperture are shown in Figure 24(a). In order to suppress the spurious backward radiation from the circular aperture, a hollow hemispherical backing cavity is placed beneath the tuning fork. In this way, an impedance bandwidth of 38% has been achieved in combination with a cylindrical DRA having relative permittivity $\epsilon_r \simeq 10$.

An alternative feeding aperture geometry which allows broadening the impedance bandwidth of a DRA is the U-shaped slot shown in Figure 24(b) [54]. This solution has the advantage of having two arms (L_A and L_C) and, therefore, an additional degree of freedom in the design and optimization of the DRA feeding. By fine-tuning the length and the width of each arm of the slot, the impedance bandwidth and/or the polarization of the antenna can be controlled. It has been shown in [54] that the length ratio of the two arms should be close to the unity in order to achieve a beneficial enhancement of the impedance bandwidth. On the other hand, a large length ratio results in a circular polarization of the antenna.

7.4. Hybrid Approach. Hybrid design approaches rely on the combination of DRAs and radiating patch/slot antennas. By tuning the resonant frequency of the radiating patch/slot antenna in order to be close to that of the combined DRA, a wide impedance bandwidth can be achieved. A hybrid DRA resulting from the combination of a ring-shaped dielectric resonator and a circular microstrip patch, fed by a resonant slot, is presented in [55] and shown in Figure 26. The measured impedance bandwidth of this hybrid DRA is such to cover the 60 GHz unlicensed frequency band from 57 GHz to 65 GHz. Another hybrid DRA design solution relying on the combination of a monopole antenna with a ring dielectric resonator is proposed in [56] (see Figure 25(a)). Such antenna structure is characterized by three main resonances. Two of such resonances are associated with the monopole and the dielectric ring resonator, respectively, whereas a third, intermediate, resonance results from the combination of the other ones. The operational frequency band of the physical prototype presented in [56] extends from 5 GHz to 13 GHz with the magnitude of the input reflection coefficient smaller than −10 dB. Similar hybrid DRAs with the dielectric ring resonator replaced by one having conical or hemispherical (see Figure 25(b)) geometry have been presented in [57]. In particular, by using a hemispherical DR, the impedance bandwidth of the radiating structure has been increased to 126%, covering in this way the frequency range between 5 GHz and 21 GHz.

A hybrid DRA combining a rectangular DR and a CPW inductive slot (see Figure 11(b)) has been introduced in [58] in order to achieve a wide-band behavior. As a matter of fact, the resonant frequencies of the rectangular DR and of the inductive slot are designed to be 5.4 GHz and 5.8 GHz, respectively, resulting in a measured impedance bandwidth of 23%, between 4.86 GHz and 6.15 GHz.

A similar design approach is adopted in [59], where a hybrid DRA resulting from the combination of a radiating inductive slot and a cylindrical DR has been proposed. The two resonances associated with the feeding slot and the dielectric resonator, respectively, result in a dual-band behavior with measured impedance bandwidths of 9% (from 3300 MHz to 3612 MHz) and 4.8% (from 4681 MHz to 4912 MHz), respectively.

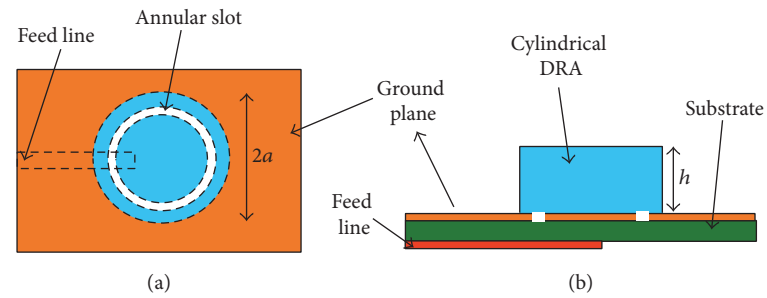

FIGURE 23: Top (a) and cross-sectional view (b) of a rectangular DRA excited by an annular slot.

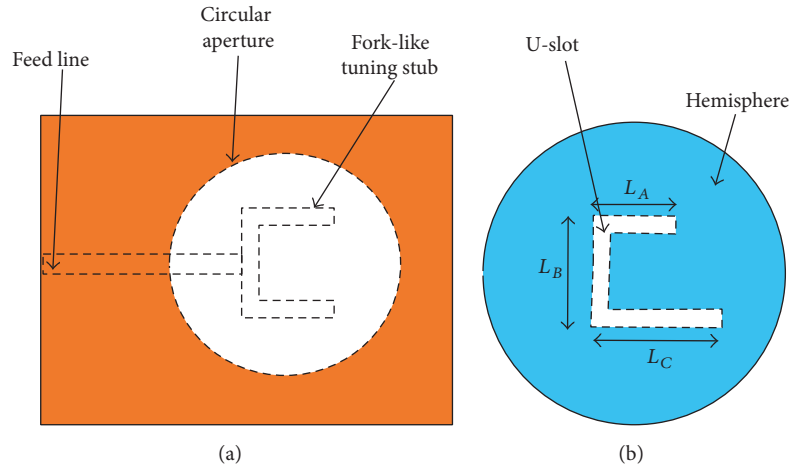

FIGURE 24: Circular aperture slot (a) as introduced in [53] and U-shaped slot (b) as investigated in [54].

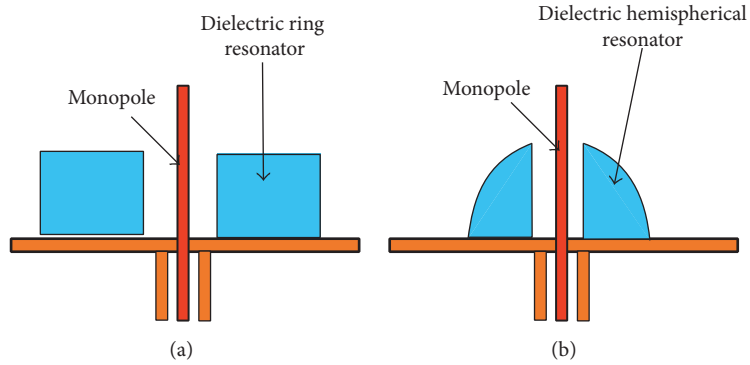

FIGURE 25: Cross-sectional view of a hybrid DRA consisting of a monopole and a ring DR (a) as suggested in [56]. Cross-sectional view of a hybrid DRA consisting of a monopole and a conical DR (b) as suggested in [57].

8. Millimeter-Wave DRAs

One of the intrinsic characteristics of DRAs is the absence of conduction losses. This property makes DRAs very suitable for high-frequency applications. In this section, major and more recent advances of DRA technology at mm-wave frequencies are summarized.

8.1. Off-Chip DRA. At millimeter-wave frequencies and beyond, the size of dielectric resonators become very small, which makes the manufacturing of the DRA challenging without resorting to expensive fabrication techniques. In order to overcome this limitation and, at the same time, improve antenna gain, electrically large DRAs exploiting higher-order modes are to be adopted.

A hybrid approach combining the excitation of higher-order modes with the radiation from the antenna feed has been presented in [55]. Figure 26 shows the top view (a) and the cross-sectional view (b) of the suggested design resulting from the combination of a ring-shaped dielectric resonator and a circular microstrip patch fed by a resonant slot. The $HEM_{15\delta}$ mode of the DRA is excited. A constant measured antenna gain of approximately 12 dBi is reported for the proposed hybrid DRA [55]. The antenna covers the 60 GHz

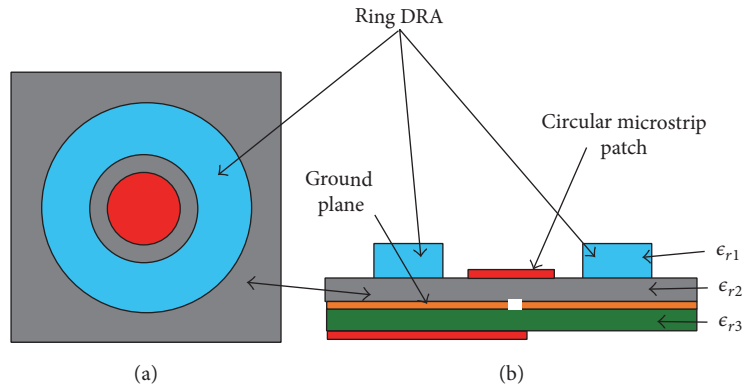

FIGURE 26: Top view (a) and cross-sectional view (b) of a hybrid ring/patch DRA as introduced in [55].

TABLE 6: Most Recent Advances in dielectric resonator antennas for millimeter-wave Applications.

Reference/Year	DRA topology	Relative permittivity	Feeding mechanism	Technology	Frequency (GHz)	Impedance bandwidth (%)	Gain (dBi)
[55]/2009	Ring with microstrip Patch	10	Coupling slot	PCB	60	15	12
[61]/2010	Cylindrical	10	Coupling slot	PCB	60	24	5.5
[62]/2011	Rectangular	10	Coupling slot	PCB	24	3.8	6.3
[63]/2011	Rectangular	10.2	Capacitive slot/CPW	PCB	60	17.4	10.2
[64]/2012	Cylindrical	10.2	Coupling slot	PCB	60	14.3	15.7
[65]/2013	Cylindrical	10.2	Coupling slot	PCB	60	22.9*	8.6
[66]/2016	Cylindrical	10.2	Coupling slot	PCB	60	10*	—
[60]/2016	Ring with microstrip Patch	10.2	Coupling slot	PCB	60	12	16.5
[67]/2007	Rectangular	48	CPW	Integrated on chip	60	2.8	3.2
[68]/2008	Cylindrical	42	Folded dipole/CPW	Integrated on chip	27.7	9.8	1
[69]/2010	Rectangular	38	H-slot/CPW	Integrated on chip	35	12	0.5
[70]/2012	Rectangular	10	Meander slot/CPW	Integrated on chip	130	12	2.7
[70]/2012	Two-layer rectangular	10	Meander slot/CPW	Integrated on chip	130	11	4.7
[71]/2013	Rectangular	12.6	Coupling slot	Integrated on chip	60.5	6.1	6
[72]/2015	Rectangular	9.8	E-shaped/CPW	Integrated on chip	340	12	10
[73]/2015	Circular	12.6	Dipole/CPW	Integrated on chip	60	3.78	7

∗ is estimated from graph.

unlicensed frequency band (from 57 GHz to 65 GHz) with a nearly flat gain of about 12 dBi. A similar concept has been recently proposed in [60] where the resonances of a circular patch and a ring-shaped DRA are combined together in order to achieve a broadband behavior while improving the antenna gain. An impedance matching bandwidth of 12% (from 57 GHz to 64 GHz) has been predicted numerically for such radiating structures. The simulated antenna gain is 16.5 dBi, this being reported as the largest gain level featured by a single-element DRA. The characteristics of the considered antenna are listed in Table 6.

A class of linearly and circularly polarized cylindrical DRAs fed by substrate integrated waveguides is presented in [61]. The proposed DRAs are designed in such a way as to resonate at 60 GHz. The measured impedance bandwidths are 24% and 4.5% for the linearly and circularly polarized DRAs, respectively. The performance characteristics of the linearly polarized DRA are summarized in Table 6.

The effect of the fabrication tolerances on the frequency shift of higher-order modes is investigated in [62] and listed in Table 7. It is clearly indicated in the table that higher-order modes are less affected by fabrication errors which is very

Table 7: Simulated frequency shift of higher order modes of a rectangular DRA due to fabrication tolerances [62].

Fabrication error (mm)	TE_{111} mode Δf (%)	TE_{115} mode Δf (%)	TE_{119} mode Δf (%)
0.01	0.38	0.21	0.12
0.05	2.04	1.00	0.74
0.1	3.99	1.83	1.41

Table 8: Comparison between the volume of DRAs excited at 24 GHz by TE_{111}, TE_{115}, and TE_{119} modes.

Resonant mode	Dimensions $a \times d \times b$ (mm)	DR volume (mm^3)
TE_{111}	$2.5 \times 2.5 \times 2.1$	13.13
TE_{115}	$4.0 \times 4.0 \times 6.1$	97.6
TE_{119}	$4.2 \times 4.2 \times 10.7$	188.75

encouraging especially for mm-wave applications where the size of the DRA becomes very small.

The reduced sensitivity of higher-order modes to fabrication errors can be readily understood by observing that a DRA driven on a higher-order mode is physically much larger as compared to the same DRA when operating on the relevant fundamental mode. In order to highlight this point, the volume of rectangular DRAs excited at the higher-order modes TE_{115} and TE_{119} is compared, in Table 8, to that of a DRA operating on the TE_{111} mode. Said DRAs are all designed in order to resonate at the frequency of 24 GHz. As it can be easily noticed in Table 8, the rectangular DRAs excited at TE_{115} and TE_{119} modes are, respectively, 7.4 and 14.4 times bulkier than the equivalent radiating structure excited at its fundamental mode. Additional characteristics of the mentioned DRA driven on the TE_{119} mode are summarized in Table 6.

The gain of a single DRA element can be further increased by placing a superstrate on the top of the DR. This approach has been suggested in [63]. A cross-sectional view of the suggested antenna topology is shown in Figure 27, where a coplanar waveguide with capacitive slot (see Figure 11(c)) is used to excite the DRA. The radiating structure proposed in [63] is designed to resonate in the 60 GHz unlicensed ISM frequency band. It has been shown, in particular, that the antenna gain can be tuned by changing the distance, ds, between the superstrate and the ground plane (see Figure 27). A large impedance bandwidth of 17.4% is obtained thanks to the combined excitation of the resonances of the DRA (fundamental and higher-order modes), as well as of the feeding slot. The integration of the superstrate allows improving the antenna gain by 9 dB as compared to a conventional DRA without superstrate. In this way, a peak gain of 14.44 dBi at 60 GHz has been achieved.

An extensive study on the effect of dielectric superstrates in combination with millimeter-wave DRAs has been reported in [64]. The considered antenna topologies are shown in Figure 28. The first antenna consists of a cylindrical

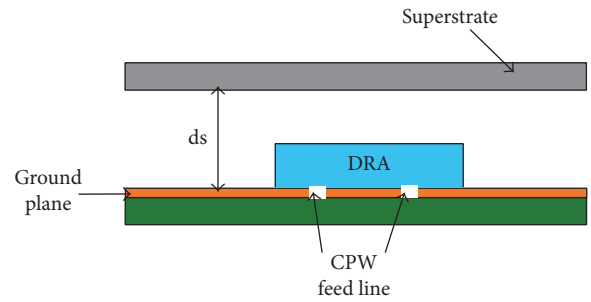

Figure 27: Rectangular DRA with superstrate for gain improvement as suggested in [63].

Table 9: Performance comparison between the DRAs shown in Figure 28.

	Antenna 1	Antenna 2	Antenna 3	Antenna 4
Impedance bandwidth (%)	36.5	14.36	13.5	14.36
Antenna gain @ 60 GHz (dBi)	6.9	7.8	14.36	15.7

DRA fed by a coupling slot (see Figure 28(a)). In the second antenna configuration (see Figure 28(b)) an intermediate substrate is integrated between the cylindrical DR and the coupling slot. By adding this dielectric layer, one gains an extra degree of freedom in the design that can be used to tune the frequency response of the DRA. The third antenna topology studied in [64] and illustrated in Figure 28(c) relies on the integration of a suitable superstrate above the DR. This concept was already presented by the same authors in [63]. The superstrate results in a focusing process of the electromagnetic field along the broadside direction of the DRA and, thanks to that, in an increase of the antenna gain [63]. The fourth antenna configuration investigated in [64] (see Figure 28(d)) is characterized by a square ring Frequency Selective Surface (FSS) printed on the superstrate. The FSS layer provides an effective means to further increase the realized gain of the antenna. The performances of the four antennas shown in Figure 28 are summarized in Table 9. It can be noticed that the integration of an intermediate dielectric substrate has a detrimental effect on the impedance bandwidth of the antenna. On the other hand, using a superstrate has a negligible impact on the bandwidth, while greatly improving the gain of the basic DRA structure. Finally, the FSS layer enables an additional gain enhancement of about 36%. The characteristics of the resulting antenna configuration 4 as shown in Figure 28(d) are summarized in Table 6.

A novel cylindrical DRA for 60 GHz applications has been presented in [65]. In such design, the dielectric resonator is surrounded by five periods of mushroom-like Electromagnetic Band Gap (EBG) elements in order to achieve a 3 dB antenna gain enhancement, while suppressing undesired surface waves.

The integration of a suitable FSS wall has been suggested in [66] in order to decrease the mutual coupling between

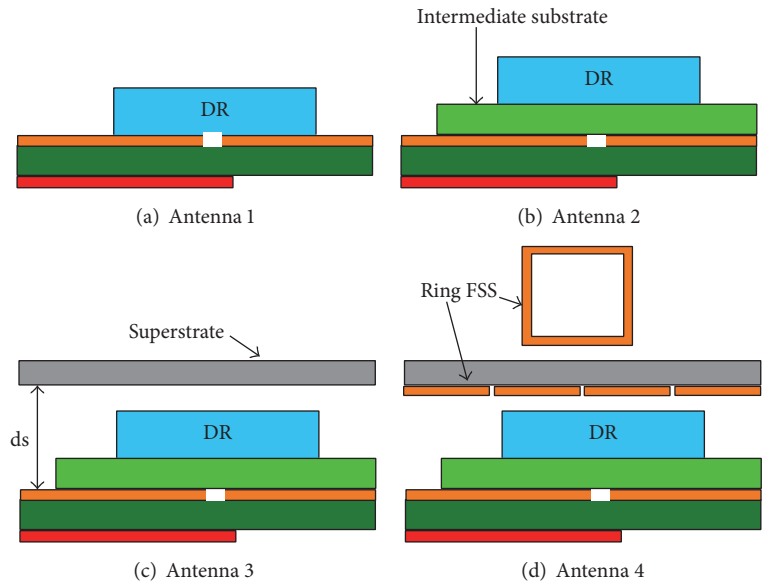

Figure 28: Millimeter-wave DRA topologies presented in [64].

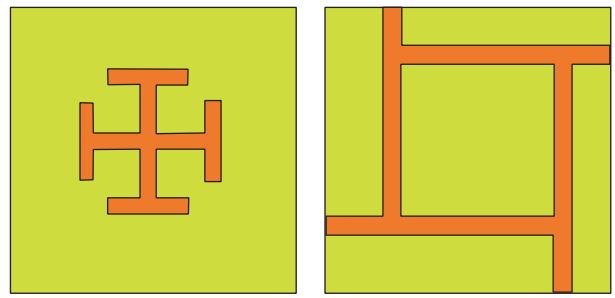

Figure 29: Front side (a) and back side (b) of the FSS unit cell useful to reduce the mutual coupling between DRAs [66].

DRAs. The proposed design is based on the combination of a Jerusalem-cross slot and a fan-like structure printed on the front and back side of the individual cell of the FSS, respectively, as shown in Figure 29. It has been proven that when such FSS wall is inserted between two cylindrical DRAs operating in the frequency band between 57 GHz and 63 GHz and placed 2.5 mm apart from each other, an 8 dB enhancement of the antenna isolation can be achieved in comparison to the identical structure without FSS wall.

8.2. On-Chip DRAs. In this section, different DRA topologies for SoC integration are reviewed. The direct integration of the antenna on chip eliminates the need of bond-wiring with a beneficial impact on manufacturing costs and miniaturization.

A 60 GHz rectangular DRA and a 27 GHz circular DRA integrated on silicon substrate are reported in [67, 68], respectively. By selecting the relative permittivity of the dielectric resonator in such a way as to be larger than the one of the silicon substrate ($\epsilon_r = 11.9$), a reduction of the fringing field effect and reduction of the losses in the substrate are achieved thanks to the focusing of the RF power toward the dielectric resonator. It has been shown that the gain and radiation efficiency of said antennas are maximum when the permittivity of DR is chosen to be $40 < \epsilon_r < 70$.

A cylindrical DRA printed on silicon substrate with 45% efficiency and 1 dBi gain is reported in [68], whereas a rectangular DRA printed on similar substrate is presented in [67]. The latter antenna shows an enhanced gain of 3.2 dBi at 60 GHz mainly thanks to the CPW feeding mechanism which isolates the DR from the lossy substrate and, at the same time, directs the radiation beam along the broadside direction. Detailed characteristics of the DRAs introduced in [67, 68] are listed in Table 6.

A rectangular DRA excited by a H-slot in CPW technology is presented in [69]. The DR is designed in such a way as to resonate at 35 GHz. The measured impedance bandwidth and radiation efficiency of such antenna are 12% and 48%, respectively.

Single- and two-layer DRAs realized in CMOS technology for applications at 130 GHz are presented in [70]. Said

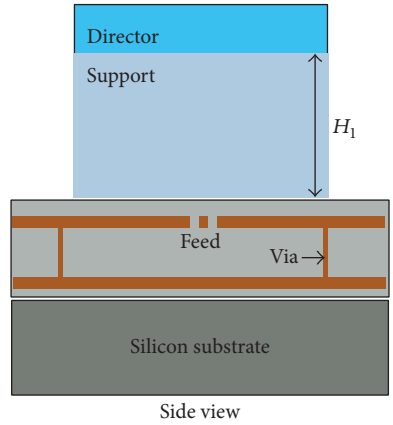

Figure 30: Side view of the suggested on-chip antenna as presented in [72].

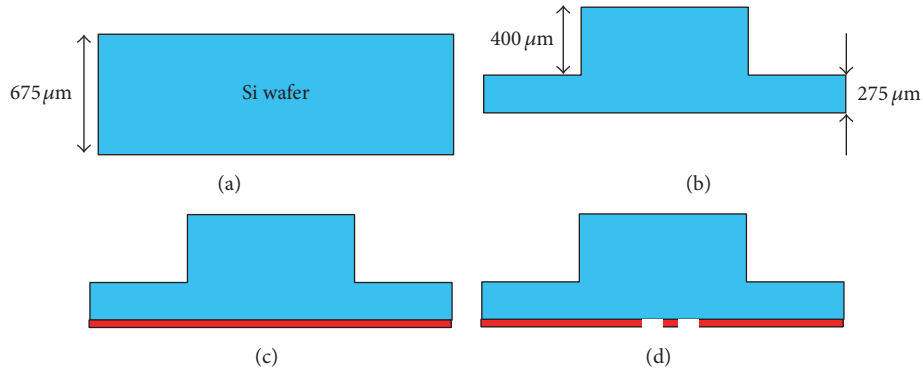

Figure 31: Manufacturing process of the DRA as suggested in [73]. (a) Single silicon wafer. (b) 400 μm etching. (c) Back side coated with copper film. (d) Back side patterned for the feeding network.

DRAs are fed by a CPW meander slot. In this way, a gain level of 2.7 dBi and 4.7 dBi has been achieved with the single-layer DRA and the stacked one, respectively. In [71] a slot-coupled rectangular DRA for mm-wave applications is presented. The relevant characteristics are summarized in Table 6.

An on-chip DRA operating at 340 GHz is presented in [72]. A Yagi-like antenna geometry is used to achieve high gain and high radiation efficiency. In order to suppress surface waves and decouple the radiator from the lossy silicon substrate, the driver, which is a Substrate Integrated Waveguide (SIW) cavity-backed antenna, is placed underneath a coplanar waveguide E-shaped patch radiator. A dielectric resonator (DR) director is kept at a suitable distance from the feed point by means of a low-permittivity mechanical support. Figure 30 shows the cross-sectional view of the proposed antenna. The relevant relative bandwidth at 10 dB return-loss level has been simulated to be 12%, ranging from 319 GHz to 360 GHz. A peak gain of 10 dBi has been measured at the central operating frequency of 340 GHz. The characteristics of the considered antenna are summarized in Table 6.

In the aforementioned on-chip DRA designs, the two main challenges are associated with the alignment of the DR to the feed, as well as the manufacturing of the DR with the prescribed shape. Recently, a cylindrical DRA realized starting from a single silicon wafer has been presented in [73]. The proposed DRA is a complete on-chip system since the DR is micromachined in a cost-effective way on the same silicon wafer. The relevant fabrication process is detailed in [73] (see Figure 31). The resulting antenna characteristics are summarized in Table 6.

9. Conclusion

Recent developments in millimeter-wave DRA technology have been presented and discussed in detail in this survey. Furthermore, useful design guidelines have been provided to RF front-end designers in order to control circuital characteristics and radiation properties of this class of antennas.

Different feeding techniques for DRAs have been first introduced, while outlining the relevant advantages and disadvantages. Furthermore, design approaches useful to achieve size reduction of DRAs have been discussed in detail. By using high permittivity materials or by placing conducting plates along specific symmetry planes of the resonator body, one can make DRAs considerably smaller. On the other hand, the gain of a DRA can be increased either by exciting the

relevant higher-order modes (electrically large DRAs), or by integrating horn-like structures.

Particular attention has been put on hybrid design techniques which rely on the combination of DRAs and radiating patch/slot antennas. In this way, the antenna impedance bandwidth can be easily tuned in such a way as to synthesize a dual-band rather than wide-band frequency response. Circular polarization of the electromagnetic field radiated by DRAs can be achieved by using various design methodologies. In this respect, the cross-shaped feeding slot-based approach provides different benefits in terms of high coupling to the DR and additional degrees of freedom to control the polarization purity (axial ratio) of the DRA, in combination with ease of manufacturing and integration.

Finally, advances in the application of DRA technology at millimeter-wave frequencies have been presented, and the most recent implementation of on-chip DRAs and off-chip DRAs has been reviewed. It has been shown that DRAs realized on silicon substrates with standard CMOS process can be characterized by good efficiency and gain, thus proving the good potential of dielectric resonator antennas for said applications.

Competing Interests

The authors declare that they have no competing interests.

Acknowledgments

This study has been carried out in the framework of the research and development program running at *the Antenna Company Nederland B.V.* For further information, please visit the Web site http://www.antennacompany.com/.

References

[1] TU/e to develop 5G technology with European grant, https://www.tue.nl/en/university/news-and-press/news/13-05-2016tue-to-develop-5g-technology-with-european-grant/.

[2] M. Simeoni, R. Cicchetti, A. Yarovoy, and D. Caratelli, "Plastic-based supershaped dielectric resonator antennas for wide-band applications," *IEEE Transactions on Antennas and Propagation*, vol. 59, no. 12, pp. 4820–4825, 2011.

[3] M. Simeoni, R. Cicchetti, A. Yarovoy, and D. Caratelli, "Super-shaped dielectric resonator antennas," in *Proceedings of the IEEE Antennas and Propagation Society International Symposium*, pp. 1–4, June 2009.

[4] M. Simeoni, R. Cicchetti, A. Yarovoy, and D. Caratelli, "Circularly polarized supershaped dielectric resonator antennas for indoor ultra wide band applications," in *Proceedings of the IEEE International Symposium on Antennas and Propagation Society*, pp. 1–4, July 2010.

[5] D. M. Pozar, *Microwave Engineering*, John Wiley & Sons, New York, NY, USA, 2012.

[6] K. M. Luk and K. W. Leung, Eds., *Dielectric Resonant Antenna*, Research Studies Press, 2003.

[7] J.-I. Moon and S.-O. Park, "Dielectric resonator antenna for dual-band PCS/IMT-2000," *Electronics Letters*, vol. 36, no. 12, pp. 1002–1003, 2000.

[8] J. F. Legier, P. Kennis, S. Toutain, and J. Citerne, "Resonant frequencies of rectangular dlekctric resonators," *IEEE Transactions on Microwave Theory and Techniques*, vol. 28, no. 9, pp. 1031–1034, 1980.

[9] R. K. Mongia, A. Ittibipoon, and M. Cuhaci, "Low profile dielectric resonator antennas using a very high permittivity material," *Electronics Letters*, vol. 30, no. 17, pp. 1362–1363, 1994.

[10] K.-L. Wong, N.-C. Chen, and H.-T. Chen, "Analysis of a Hemispherical dielectric resonator antenna with an airgap," *IEEE Microwave and Guided Wave Letters*, vol. 3, no. 10, pp. 355–357, 1993.

[11] K. W. Leung, X. S. Fang, Y. M. Pan, E. H. Lim, K. M. Luk, and H. P. Chan, "Dual-function radiating glass for antennas and light covers—part II: dual-band glass dielectric resonator antennas," *IEEE Transactions on Antennas and Propagation*, vol. 61, no. 2, pp. 587–597, 2013.

[12] A. Petosa, A. Ittipiboon, and M. Cuhaci, "Array of circular-polarised cross dielectric resonator antennas," *Electronics Letters*, vol. 32, no. 19, pp. 1742–1743, 1996.

[13] M. Akbari, S. Gupta, R. Movahedinia, S. Zarbakhsh, and A. R. Sebak, "Bandwidth enhancement of 4×4 subarrays circularly polarized rectangular dielectric resonator antenna by sequential feeding network," in *Proceedings of the 10th European Conference on Antennas and Propagation (EuCAP '16)*, pp. 1–4, Davos, Switzerland, April 2016.

[14] M. W. McAllister, S. A. Long, and G. L. Conway, "Rectangular dielectric resonator antenna," in *Proceedings of the International Symposium Digest—Antennas and Propagation*, vol. 21, pp. 696–699, May 1983.

[15] K. W. Leung, K. M. Luk, K. Y. A. Lai, and D. Lin, "Theory and experiment of a coaxial probe fed hemispherical dielectric resonator antenna," *IEEE Transactions on Antennas and Propagation*, vol. 41, no. 10, pp. 1390–1398, 1993.

[16] R. A. Kranenburg and S. A. Long, "Microstrip transmission line excitation of dielectric resonator antennas," *Electronics Letters*, vol. 24, no. 18, pp. 1156–1157, 1988.

[17] L.-N. Zhang, S.-S. Zhong, and S.-Q. Xu, "Broadband U-shaped dielectric resonator antenna with elliptical patch feed," *Electronics Letters*, vol. 44, no. 16, pp. 947–949, 2008.

[18] R. A. Kranenburg, S. A. Long, and J. T. Williams, "Coplanar waveguide excitation of dielectric resonator antennas," *IEEE Transactions on Antennas and Propagation*, vol. 39, no. 1, pp. 119–122, 1991.

[19] B. Ghosh, K. Ghosh, and C. S. Panda, "Coplanar waveguide feed to the hemispherical DRA," *IEEE Transactions on Antennas and Propagation*, vol. 57, no. 5, pp. 1566–1570, 2009.

[20] K.-W. Leung, K.-M. Luk, K. Y. A. Lai, and D. Lin, "Theory and experiment of an aperture-coupled hemispherical dielectric resonator antenna," *IEEE Transactions on Antennas and Propagation*, vol. 43, no. 11, pp. 1192–1198, 1995.

[21] Y. M. Pan and S. Y. Zheng, "A low-profile stacked dielectric resonator antenna with high-gain and wide bandwidth," *IEEE Antennas and Wireless Propagation Letters*, vol. 15, pp. 68–71, 2016.

[22] A. A. Kishk and W. Huang, "Use of electric and magnetic conductors to reduce the DRA size," in *Proceedings of the IEEE International Workshop on Antenna Technology: Small and Smart Antennas Metamaterials and Applications (iWAT '07)*, pp. 143–146, IEEE, Cambridge, UK, March 2007.

[23] M. T. K. Tam and R. D. Murch, "Half volume dielectric resonator antenna designs," *Electronics Letters*, vol. 33, no. 23, pp. 1914–1916, 1997.

[24] A. A. Kishk and W. Huang, "Size-reduction method for dielectric-resonator antennas," *IEEE Antennas and Propagation Magazine*, vol. 53, no. 2, pp. 26–38, 2011.

[25] Nasimuddin and K. P. Esselle, "Antennas with dielectric resonators and surface mounted short horns for high gain and large bandwidth," *IET Microwaves, Antennas and Propagation*, vol. 1, no. 3, pp. 723–728, 2007.

[26] T. A. Denidni, Y. Coulibaly, and H. Boutayeb, "Hybrid dielectric resonator antenna with circular mushroom-like structure for gain improvement," *IEEE Transactions on Antennas and Propagation*, vol. 57, no. 4, pp. 1043–1049, 2009.

[27] R. Cicchetti, A. Faraone, E. Miozzi, R. Ravanelli, and O. Testa, "A high-gain mushroom-shaped dielectric resonator antenna for wideband wireless applications," *IEEE Transactions on Antennas and Propagation*, vol. 64, no. 7, pp. 2848–2861, 2016.

[28] A. Petosa, S. Thirakoune, and A. Ittipiboon, "Higher-order modes in rectangular DRAs for gain enhancement," in *Proceedings of the 13th International Symposium on Antenna Technology and Applied Electromagnetics and the Canadian Radio Sciences Meeting (ANTEM/URSI '09)*, pp. 1–4, February 2009.

[29] L. Zhong, J. S. Hong, and H. C. Zhou, "A novel pattern-reconfigurable cylindrical dielectric resonator antenna with enhanced gain," *IEEE Antennas and Wireless Propagation Letters*, vol. 15, pp. 1253–1256, 2016.

[30] M. Mrnka and Z. Raida, "Enhanced-gain dielectric resonator antenna based on the combination of higher-order modes," *IEEE Antennas and Wireless Propagation Letters*, vol. 15, pp. 710–713, 2016.

[31] G. Drossos, Z. Wu, and L. E. Davis, "Circular polarised cylindrical dielectric resonator antenna," *Electronics Letters*, vol. 32, no. 4, pp. 281–283, 1996.

[32] K. W. Leung, W. C. Wong, K. M. Luk, and E. K. N. Yung, "Circular-polarised dielectric resonator antenna excited by dual conformal strips," *Electronics Letters*, vol. 36, no. 6, pp. 484–486, 2000.

[33] M. T. K. Tam and R. D. Murch, "Circularly polarized circular sector dielectric resonator antenna," *IEEE Transactions on Antennas and Propagation*, vol. 48, no. 1, pp. 126–128, 2000.

[34] M. B. Oliver, Y. M. M. Antar, R. K. Mongia, and A. Ittipiboon, "Circularly polarised rectangular dielectric resonator antenna," *Electronics Letters*, vol. 31, no. 6, pp. 418–419, 1995.

[35] K. P. Esselle, "Circularly polarised higher-order rectangular dielectric-resonator antenna," *Electronics Letters*, vol. 32, no. 3, pp. 150–151, 1996.

[36] S. Fakhte, H. Oraizi, and R. Karimian, "A novel low-cost circularly polarized rotated stacked dielectric resonator antenna," *IEEE Antennas and Wireless Propagation Letters*, vol. 13, pp. 722–725, 2014.

[37] M. Zou and J. Pan, "Wide dual-band circularly polarized stacked rectangular dielectric resonator antenna," *IEEE Antennas and Wireless Propagation Letters*, vol. 15, pp. 1140–1143, 2015.

[38] G. Almpanis, C. Fumeaux, and R. Vahldieck, "Offset cross-slot-coupled dielectric resonator antenna for circular polarization," *IEEE Microwave and Wireless Components Letters*, vol. 16, no. 8, pp. 461–463, 2006.

[39] A. Laisné, R. Gillard, and G. Piton, "Circularly polarised dielectric resonator antenna with metallic strip," *Electronics Letters*, vol. 38, no. 3, pp. 106–107, 2002.

[40] K. W. Leung, W. C. Wong, and H. K. Ng, "Circularly polarized slot-coupled dielectric resonator antenna with a parasitic patch," *IEEE Antennas and Wireless Propagation Letters*, vol. 1, no. 1, pp. 57–59, 2002.

[41] B. Li and K. W. Leung, "Strip-fed rectangular dielectric resonator antennas with/without a parasitic patch," *IEEE Transactions on Antennas and Propagation*, vol. 53, no. 7, pp. 2200–2207, 2005.

[42] R. Chair, S. L. S. Yang, A. A. Kishk, K. F. Lee, and K. M. Luk, "Aperture fed wideband circularly polarized rectangular stair shaped dielectric resonator antenna," *IEEE Transactions on Antennas and Propagation*, vol. 54, no. 4, pp. 1350–1352, 2006.

[43] R. Chair, A. A. Kish, and K. F. Lee, "Wideband stair-shaped dielectric resonator antennas," *IET Microwaves, Antennas and Propagation*, vol. 1, no. 2, pp. 299–305, 2007.

[44] W. Huang and A. A. Kishk, "Compact dielectric resonator antenna for microwave breast cancer detection," *IET Microwaves, Antennas and Propagation*, vol. 3, no. 4, pp. 638–644, 2009.

[45] P. Gupta, D. Guha, and C. Kumar, "Dielectric resonator working as feed as well as antenna: new concept for dual-mode dual-band improved design," *IEEE Transactions on Antennas and Propagation*, vol. 64, no. 4, pp. 1497–1502, 2016.

[46] R. Chair, A. A. Kishk, and K. F. Lee, "Experimental investigation for wideband perforated dielectric resonator antenna," *Electronics Letters*, vol. 42, no. 3, pp. 137–139, 2006.

[47] T. A. Denidni and Z. Weng, "Rectangular dielectric resonator antenna for ultrawideband applications," *Electronics Letters*, vol. 45, no. 24, pp. 1210–1212, 2009.

[48] M. Khalily, M. K. A. Rahim, and A. A. Kishk, "Bandwidth enhancement and radiation characteristics improvement of rectangular dielectric resonator antenna," *IEEE Antennas and Wireless Propagation Letters*, vol. 10, pp. 393–395, 2011.

[49] Z. Fan and Y. M. M. Antar, "Slot-coupled DR antenna for dual-frequency operation," *IEEE Transactions on Antennas and Propagation*, vol. 45, no. 2, pp. 306–308, 1997.

[50] S. Dhar, R. Ghatak, B. Gupta, and D. R. Poddar, "A wideband Minkowski fractal dielectric resonator antenna," *IEEE Transactions on Antennas and Propagation*, vol. 61, no. 6, pp. 2895–2903, 2013.

[51] B. Mukherjee, P. Patel, and J. Mukherjee, "A novel cup-shaped inverted hemispherical dielectric resonator antenna for wideband applications," *IEEE Antennas and Wireless Propagation Letters*, vol. 12, pp. 1240–1243, 2013.

[52] K. W. Leung, W. C. Wong, K. M. Luk, and E. K. N. Yung, "Annular slot-coupled dielectric resonator antenna," *Electronics Letters*, vol. 34, no. 13, pp. 1275–1277, 1998.

[53] K. W. Leung and C. K. Leung, "Wideband dielectric resonator antenna excited by cavity-backed circular aperture with microstrip tuning fork," *Electronics Letters*, vol. 39, no. 14, pp. 1033–1035, 2003.

[54] H. Y. Lam and K. W. Leung, "Analysis of U-slot-excited dielectric resonator antennas with a backing cavity," *IEE Proceedings—Microwaves, Antennas and Propagation*, vol. 153, no. 5, pp. 480–482, 2006.

[55] A. Perron, T. A. Denidni, and A.-R. Sebak, "High-gain hybrid dielectric resonator antenna for millimeter-wave applications: design and implementation," *IEEE Transactions on Antennas and Propagation*, vol. 57, no. 10, pp. 2882–2892, 2009.

[56] D. Guha, Y. M. M. Antar, A. Ittipiboon, A. Petosa, and D. Lee, "Improved design guidelines for the ultra wideband monopole-dielectric resonator antenna," *IEEE Antennas and Wireless Propagation Letters*, vol. 5, no. 1, pp. 373–376, 2006.

[57] D. Guha, B. Gupta, and Y. M. M. Antar, "Hybrid monopole-DRAs using hemispherical/conical-shaped dielectric ring resonators: improved ultrawideband designs," *IEEE Transactions on Antennas and Propagation*, vol. 60, no. 1, pp. 393–398, 2012.

[58] Y. Gao, A. P. Popov, B. L. Ooi, and M. S. Leong, "Experimental study of wideband hybrid dielectric resonator antenna on small ground plane," *Electronics Letters*, vol. 42, no. 13, pp. 731–733, 2006.

[59] Y.-F. Lin, H.-M. Chen, and C.-H. Lin, "Compact dual-band hybrid dielectric resonator antenna with radiating slot," *IEEE Antennas and Wireless Propagation Letters*, vol. 8, pp. 6–9, 2009.

[60] E. Erfani, T. Denidni, S. Tatu, and M. Niroo-Jazi, "A broadband and high gain millimeter-wave hybrid dielectric resonator antenna," in *Proceedings of the 17th International Symposium on Antenna Technology and Applied Electromagnetics (ANTEM '16)*, pp. 1–2, IEEE, Montreal, Canada, July 2016.

[61] Q. Lai, C. Fumeaux, W. Hong, and R. Vahldieck, "60 GHz aperture-coupled dielectric resonator antennas fed by a half-mode substrate integrated waveguide," *IEEE Transactions on Antennas and Propagation*, vol. 58, no. 6, pp. 1856–1864, 2010.

[62] Y.-M. Pan, K. W. Leung, and K.-M. Luk, "Design of the millimeter-wave rectangular dielectric resonator antenna using a higher-order mode," *IEEE Transactions on Antennas and Propagation*, vol. 59, no. 8, pp. 2780–2788, 2011.

[63] Y. Coulibaly, M. Nedil, I. Ben Mabrouk, L. Talbi, and T. A. Denidni, "High gain rectangular dielectric resonator for broadband millimeter-waves underground communications," in *Proceedings of the 24th Canadian Conference on Electrical and Computer Engineering (CCECE '11)*, pp. 001088–001091, IEEE, Ontario, Canada, May 2011.

[64] Y. Coulibaly, M. Nedil, L. Talbi, and T. A. Denidni, "Design of high gain and broadband antennas at 60 GHz for underground communications systems," *International Journal of Antennas and Propagation*, vol. 2012, Article ID 386846, 7 pages, 2012.

[65] M. J. Al-Hasan, T. A. Denidni, and A. R. Sebak, "Millimeter-wave EBG-based aperture-coupled dielectric resonator antenna," *IEEE Transactions on Antennas and Propagation*, vol. 61, no. 8, pp. 4354–4357, 2013.

[66] R. Karimian, A. Kesavan, M. Nedil, and T. A. Denidni, "Low mutual coupling 60-GHz MIMO antenna system with frequency selective surface wall," *IEEE Antennas and Wireless Propagation Letters*, 2016.

[67] P. V. Bijumon, Y. M. M. Antar, A. P. Freundorfer, and M. Sayer, "Integrated dielectric resonator antennas for system on-chip applications," in *Proceedings of the International Conference on Microelectronics (ICM '07)*, pp. 275–278, IEEE, Cairo, Egypt, December 2007.

[68] P. V. Bijumon, Y. M. M. Antar, A. P. Freundorfer, and M. Sayer, "Dielectric resonator antenna on silicon substrate for system on-chip applications," *IEEE Transactions on Antennas and Propagation*, vol. 56, no. 11, pp. 3404–3410, 2008.

[69] M.-R. Nezhad-Ahmadi, M. Fakharzadeh, B. Biglarbegian, and S. Safavi-Naeini, "High-efficiency on-chip dielectric resonator antenna for mm-wave transceivers," *IEEE Transactions on Antennas and Propagation*, vol. 58, no. 10, pp. 3388–3392, 2010.

[70] D. Hou, Y.-Z. Xiong, W.-L. Goh, S. Hu, W. Hong, and M. Madihian, "130-GHz on-chip meander slot antennas with stacked dielectric resonators in standard CMOS technology," *IEEE Transactions on Antennas and Propagation*, vol. 60, no. 9, pp. 4102–4109, 2012.

[71] L. Ohlsson, T. Bryllert, C. Gustafson et al., "Slot-coupled millimeter-wave dielectric resonator antenna for high-efficiency monolithic integration," *IEEE Transactions on Antennas and Propagation*, vol. 61, no. 4, pp. 1599–1607, 2013.

[72] X.-D. Deng, Y. Li, C. Liu, W. Wu, and Y.-Z. Xiong, "340 GHz On-Chip 3-D antenna with 10 dBi Gain and 80% radiation efficiency," *IEEE Transactions on Terahertz Science and Technology*, vol. 5, no. 4, pp. 619–627, 2015.

[73] M. O. Sallam, M. Serry, S. Sedky et al., "Micromachined on-chip dielectric resonator antenna operating at 60 GHz," *IEEE Transactions on Antennas and Propagation*, vol. 63, no. 8, pp. 3410–3416, 2015.